AD-A047 566 ARMY ELECTRONICS COMMAND FORT MONMOUTH N J F/G 9/5
ELECTRONIC MEASUREMENT OF CRYSTAL RESONATOR TEMPERATURE ANOMALI--ETC(U)
AUG 77 A BALLATO, R TILTON

UNCLASSIFIED ECOM-4516 NL

| OF |
AD
A047 566

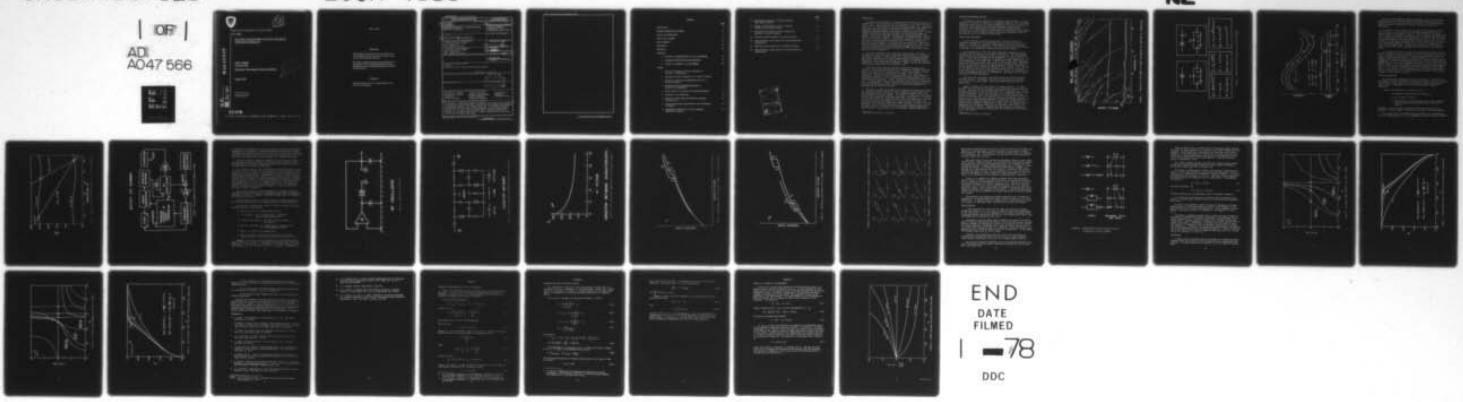

END
DATE
FILMED
-78
DDC

Research and Development Technical Report

ECOM -4516

ELECTRONIC MEASUREMENT OF CRYSTAL RESONATOR TEMPERATURE ANOMALIES

Arthur Ballato
Richard Tilton

Electronics Technology & Devices Laboratory

August 1977

ECOM

US ARMY ELECTRONICS COMMAND FORT MONMOUTH, NEW JERSEY 07703

NOTICES

Disclaimers

The findings in this report are not to be construed as an official Department of the Army position, unless so designated by other authorized documents.

The citation of trade names and names of manufacturers in this report is not to be construed as official Government indorsement or approval of commercial products or services referenced herein.

Disposition

Destroy this report when it is no longer needed. Do not return it to the originator.

UNCLASSIFIED
SECURITY CLASSIFICATION OF THIS PAGE (When Data Entered)

REPORT DOCUMENTATION PAGE

READ INSTRUCTIONS BEFORE COMPLETING FORM

1. REPORT NUMBER: ECOM-4516
2. GOVT ACCESSION NO.
3. RECIPIENT'S CATALOG NUMBER

4. TITLE (and Subtitle): ELECTRONIC MEASUREMENT OF CRYSTAL RESONATOR TEMPERATURE ANOMALIES.
5. TYPE OF REPORT & PERIOD COVERED: Technical Report, August 1977
6. PERFORMING ORG. REPORT NUMBER

7. AUTHOR(s): Arthur/Ballato [redacted] Richard/Tilton
8. CONTRACT OR GRANT NUMBER(s)

9. PERFORMING ORGANIZATION NAME AND ADDRESS:
US Army Electronics Command
ATTN: DRSEL-TL-ML
Fort Monmouth, NJ 07703
10. PROGRAM ELEMENT, PROJECT, TASK AREA & WORK UNIT NUMBERS: 1T1 61101 A 91A 09 455

11. CONTROLLING OFFICE NAME AND ADDRESS:
US Army Electronics Command
ATTN: DRSEL-TL-ML
Fort Monmouth, NJ 07703
12. REPORT DATE: Aug[redacted]977
13. NUMBER OF PAGES: 29 (34p.)

14. MONITORING AGENCY NAME & ADDRESS (if different from Controlling Office)
15. SECURITY CLASS. (of this report): UNCLASSIFIED
15a. DECLASSIFICATION/DOWNGRADING SCHEDULE

16. DISTRIBUTION STATEMENT (of this Report)
Statement A.
Approved for public release; distribution unlimited.

037 620

17. DISTRIBUTION STATEMENT (of the abstract entered in Block 20, if different from Report)

DDC RECEIVED DEC 14 1977 F

18. SUPPLEMENTARY NOTES

19. KEY WORDS (Continue on reverse side if necessary and identify by block number)

Piezoelectric vibrators	Crystal oscillators	Activity dips
Piezoelectric crystals	Automatic Test Equipment	Bandbreaks
Transducers	Activity Anomalies	Frequency Control
Crystal resonators	Temperature Anomalies	

20. ABSTRACT (Continue on reverse side if necessary and identify by block number)

The frequency- or immittance-temperature anomalies occurring in quartz crystal resonators are called activity dips. Testing for their presence can represent a considerable addition to the manufacturing cost. An electronic method is described that is rapid, simple, and well adapted to microprocessor control. It makes use of the fact that the desired mode of vibration is shifted in frequency by a variable series capacitor, while interfering modes that cause activity dips are nearly unaffected.

DD FORM 1 JAN 73 1473 EDITION OF 1 NOV 65 IS OBSOLETE

UNCLASSIFIED
SECURITY CLASSIFICATION OF THIS PAGE (When Data Entered)

CONTENTS

INTRODUCTION

Anomalies in the frequency- or admittance-temperature characteristic of a resonator are called "activity dips" or "bandbreaks." At least two distinct species exist: "design-related" dips and "process-related" dips. The latter type arise from shortcomings in the processing phases where, for example, an improperly deposited electrode film peels or blisters in a reversible, temperature-dependent manner; these are not considered further here. "Design-related" activity dips are those for which the structural configuration remains unaffected by temperature changes, but instead depend solely upon geometry and material constants. The presence of "design-related" activity dips is a persistent problem and necessitates a good deal of costly testing for medium- and high-precision resonator units.[1-6]* Doubly rotated cuts generally could be expected to have even more problems in this regard than AT-cuts since they exhibit less symmetry and have, therefore, a more complicated mode spectrum when lateral boundaries are taken into account. An exception appears to be the SC/TTC orientation[7-10]* for which activity dips have yet to be encountered.[11]*

The modal interference that takes place may be linear or nonlinear. If the impressed voltage can drive the desired thickness mode and at the same time drive a harmonic of flexural mode, e.g., then the vibrator admittance will reflect this fact as the linear superposition of the separate modal admittances. With temperature changes it is possible for the two resonance frequencies to cross and produce an anomaly. Linear activity dips have been described by Wood and Seed[4] and by Fukuyo et al.[2]

Nonlinear activity dips are less well understood and perhaps more important. Wood and Seed[4] found the AT-cut fundamental thickness shear frequency to be affected by interfering modes at twice its frequency; Franx[3] observed the same type of coupling due to a mode at three times the fundamental. Birch and Weston[6] investigated both cases. Koga[5] found the twenty-first harmonic of contour extension interfering nonlinearly with the thickness shear fundamental. Similar results were obtained by Fukuyo et al.[2] In all cases the sensitivity of mode coupling to power levels is a characteristic of nonlinearity. Hafner[1] found that the anomalies encountered at the fifth and seventh harmonics were nonlinear in nature and depended on the electrode film as well as the quartz.

The effect of inserting a capacitor in series with a crystal is to shift all resonance frequencies upward by amounts roughly inversely proportional to the capacitance ratios of the modes. The temperature coefficients of the various modes are similarly altered. As a result of these facts, and because the interfering modes have differing temperature coefficients, it is possible to alter the activity dip temperature by a series load capacitance. By using an adjustable capacitance network, the activity dip spectrum may be electronically swept while the temperature remains constant. In effect, the time-consuming, costly, frequency-temperature oven runs presently used for detecting activity dips are replaced by an all-electronic constant-temperature procedure that is rapid, simple, and well adapted to microprocessor control.

* See list of references on Page 23.

FREQUENCY-TEMPERATURE SPECTRUM

In Figure 1 we show a portion of the unwanted mode spectrum of a quartz resonator, as function of temperature, obtained by Fukuyo et al.[2] This painstaking work shows clearly how various responses may drift into coincidence at particular temperatures due to differing temperature coefficients of frequency. The responses shown are those detected piezoelectrically. It is also possible to drive indirectly nonpiezoelectric modes that would not appear on such a chart and yet whose presences could produce anomalies. This is particularly true of nonlinearly coupled modes.

SERIES LOAD CAPACITANCE

In the vicinity of the main desired mode, a crystal resonator is adequately represented by the Butterworth-Van Dyke equivalent circuit in Figure 2. The effect of inserting a load capacitor C_L in series with the crystal may also be represented by a circuit of the same form, but with modified values. The appropriate formulas are also given in Figure 2.

The important fact is that the crystal resonance frequency $f_R \simeq f_S$ is shifted by the load capacitor to a higher frequency f_L. The load frequency f_L depends upon C_L through the fraction α, and upon the crystal capacitance ratio r. For an AT-cut operated at the fundamental, a typical value for r is 250, so that f_L could be pulled up to 2,000 ppm by extreme changes in C_L. An interfering mode, on the other hand, is apt to have a very large capacitance ratio, and so would be shifted very little by the presence of C_L. This would be the case with modes such as the high overtones of flexure;[12]* nonpiezoelectric modes would be completely unaffected by the presence of C_L. Because of the effective capacitance of the thickness modes, such as the desired AT-cut shear mode, varies with the square of the harmonic, the overtones will shift correspondingly less than the fundamental. The same is true of their nonlinearly produced subharmonics.

The series load capacitance thus shifts upward the different modes by different amounts. Accordingly, the points of intersection of the modes (cf. Figure 1) will also change. This is the basis upon which the test method rests.

Figure 3 contains "hot plots" made of a 20 MHz resonator. The upper S-shaped curves are plots of frequency versus temperature, and are typical of AT-cuts. The lowest S-curve was measured without C_L and labeled f_R. It has an anomaly marked by an arrow at about 78°C. The corresponding curve of grid current (proportional to the crystal admittance) is marked R_R, and also exhibits an anomaly. When a load capacitor C_{L1} is placed in series with the crystal in the oscillator, the curves f_{L1} and R_{L1} are produced. Now the activity dip has been displaced downward in temperature to approximately 58°C. Substitution of a smaller capacitor C_{L2} is seen to shift the activity dip anomaly further downward in temperature to about 44°C. The downward shift in temperature for the anomaly means that the temperature coefficient of the interfering mode is negative. Assuming that the resonator in question had r = 250 would mean that the interfering mode had a temperature coefficient of about -5.6×10^{-6}/K.

---

* See list of references on Page 23.

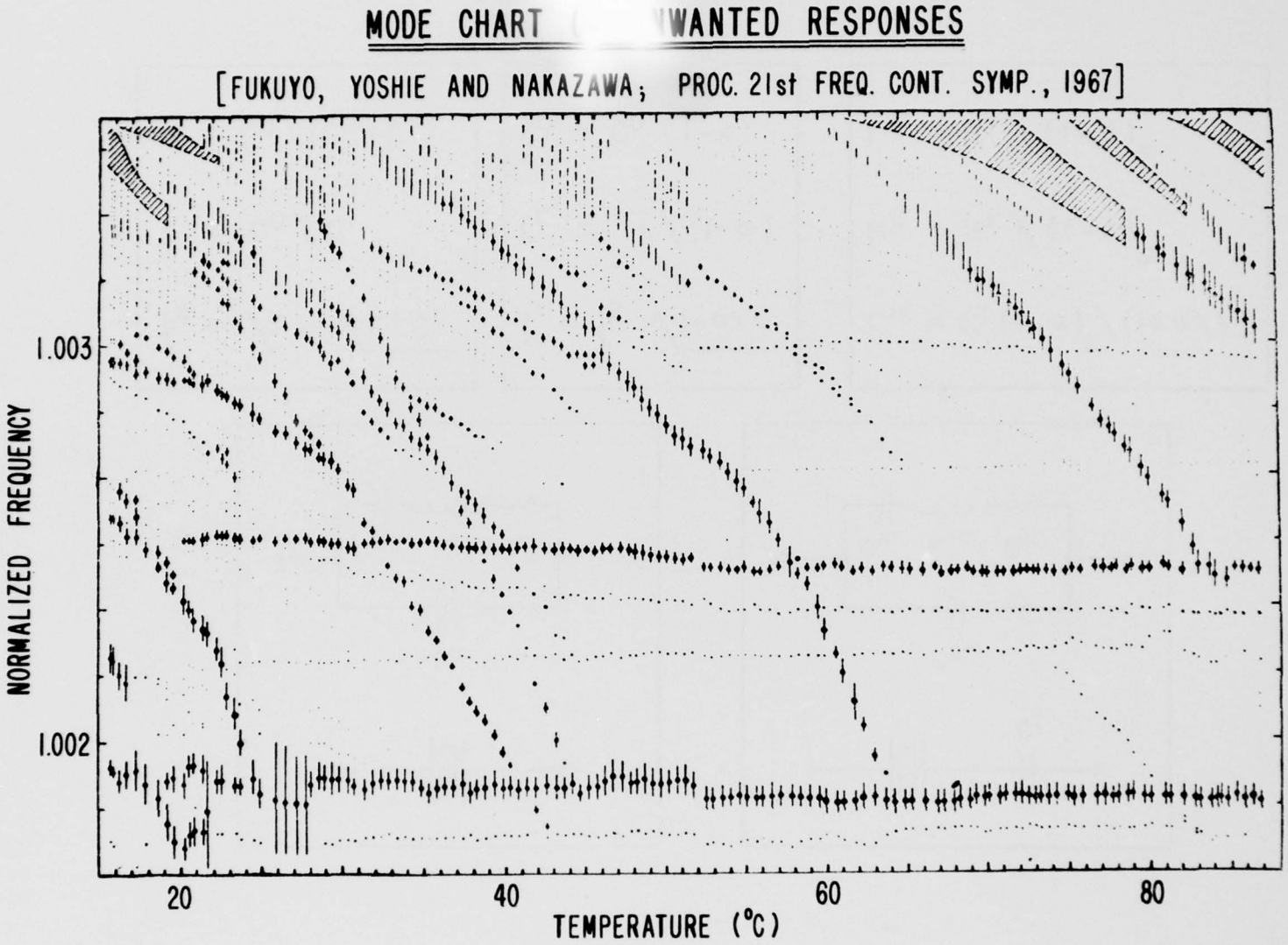

FIGURE 1. PORTION OF SPECTRUM OF QUARTZ RESONATOR AS FUNCTION OF TEMPERATURE.

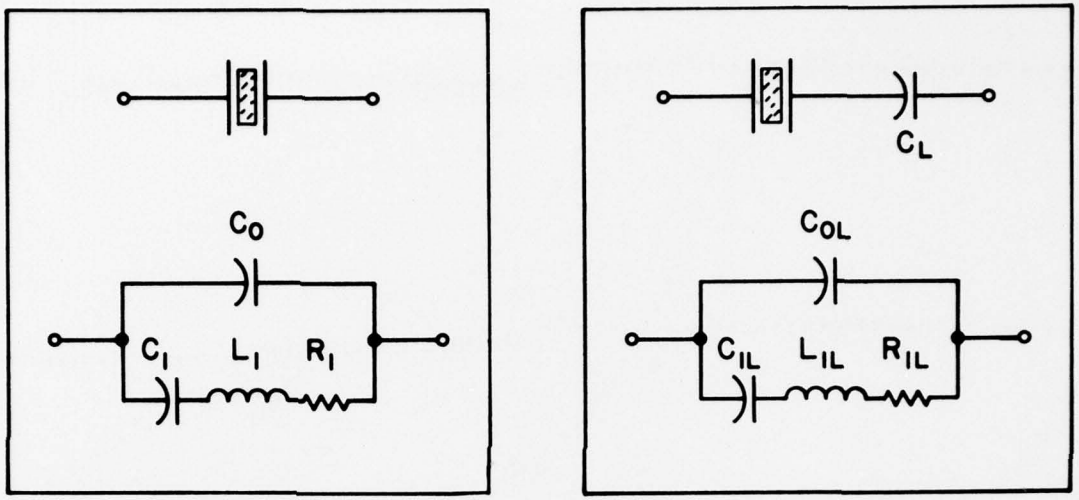

$$f_s = 1/2\pi\sqrt{L_1 C_1}$$

$$r = C_0 / C_1$$

$$\alpha = C_0 / (C_0 + C_L)$$

$$f_L = f_s \sqrt{1+\alpha/r}$$

$$r_L \simeq r/(1-\alpha)$$

$$C_{OL} = C_0 (1-\alpha)$$

$$C_{IL} = C_1 (1-\alpha)^2 / (1+\alpha/r)$$

$$R_{IL} = R_1 / (1-\alpha)^2$$

$$L_{IL} = L_1 / (1-\alpha)^2$$

FIGURE 2. EQUIVALENT CIRCUIT PARAMETERS OF A CRYSTAL VIBRATOR.

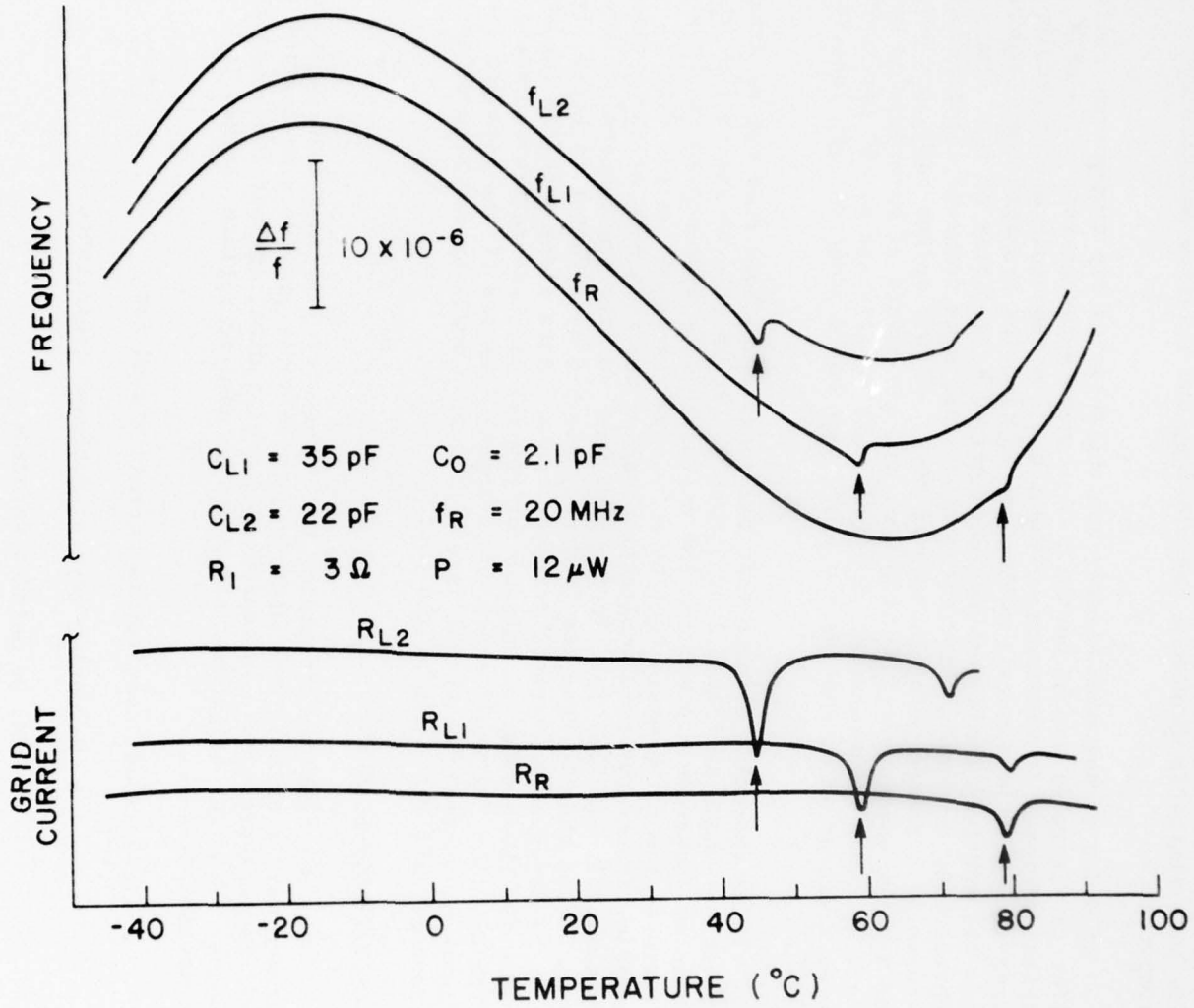

FIGURE 3. FREQUENCY- AND ACTIVITY-TEMPERATURE PLOTS OF A CRYSTAL RESONATOR.

The $\Delta f/f$ scale provided on Figure 3 pertains to each of the S-curves individually; the vertical separation between S-curves has been greatly reduced so that they could be compared more easily. The resistance curves have been similarly displaced for clarity, and relative position is unimportant.

In order to see more clearly how the activity dip temperature shifts refer to Figure 4; at the bottom is a frequency-temperature curve of a crystal vibrator at resonance, without C_L. On the scale of the drawing, the curve is nearly horizontal; so to keep in mind its S-shaped familiar character, its vertical scale has been exaggerated by a factor of ten. Two curves representing unwanted, interfering modes have been drawn to intersect the S-curve at a common point located at 80°C. With a series capacitor attached, the S-curve moves upward by 2000 ppm, and the points of intersection now occur at lower temperatures. The mode with coefficient of -60 ppm/K produces a dip at 48°C, and the -20 ppm/K mode would produce a dip instead at -23°C.

It is important to note that the interfering mode need not be actually present as shown in Figure 1 or Figure 4. It is only necessary that the harmonic or subharmonic producing the disturbance be represented as shown in Figure 4; the curve would thus be a "virtual response" on the figure. For example, Franx[3] observed nonlinear coupling due to a mode at three times the fundamental. If this interfering mode were to have its temperature behavior mapped, and then to have its frequency divided by a factor of three, it could then be drawn as a "virtual response" on a figure along with the fundamental curve for the purpose of determining how the dip temperature would change with C_L. The "virtual" curve would appear like one of the straight lines in Figure 4, whereas the actual interfering mode would appear at some harmonic frequency off the scale of the plot.

ACTIVITY DIP SCANNER

Our observations concerning the effects of putting a load capacitor in series with a crystal resonator in an oscillator provide a method for trading off temperature scans, in search of activity dips, against load capacitor scans. That is, adjustment of C_L can be used to replace changes in temperature.

A series load capacitor is currently used for:

- Measuring crystal motional capacitance C_1;
- FM, by using a varactor;
- Compensating the frequency-temperature crystal characteristic in temperature-compensated crystal oscillators (TCXO's).

We propose to use the effect to permit electronic scanning of activity anomalies. A block diagram of an activity dip scanner is shown in Figure 5.

The program control and signal processing (PCSP) block is implemented either by a microprocessor or by a programmable calculator and data interface.

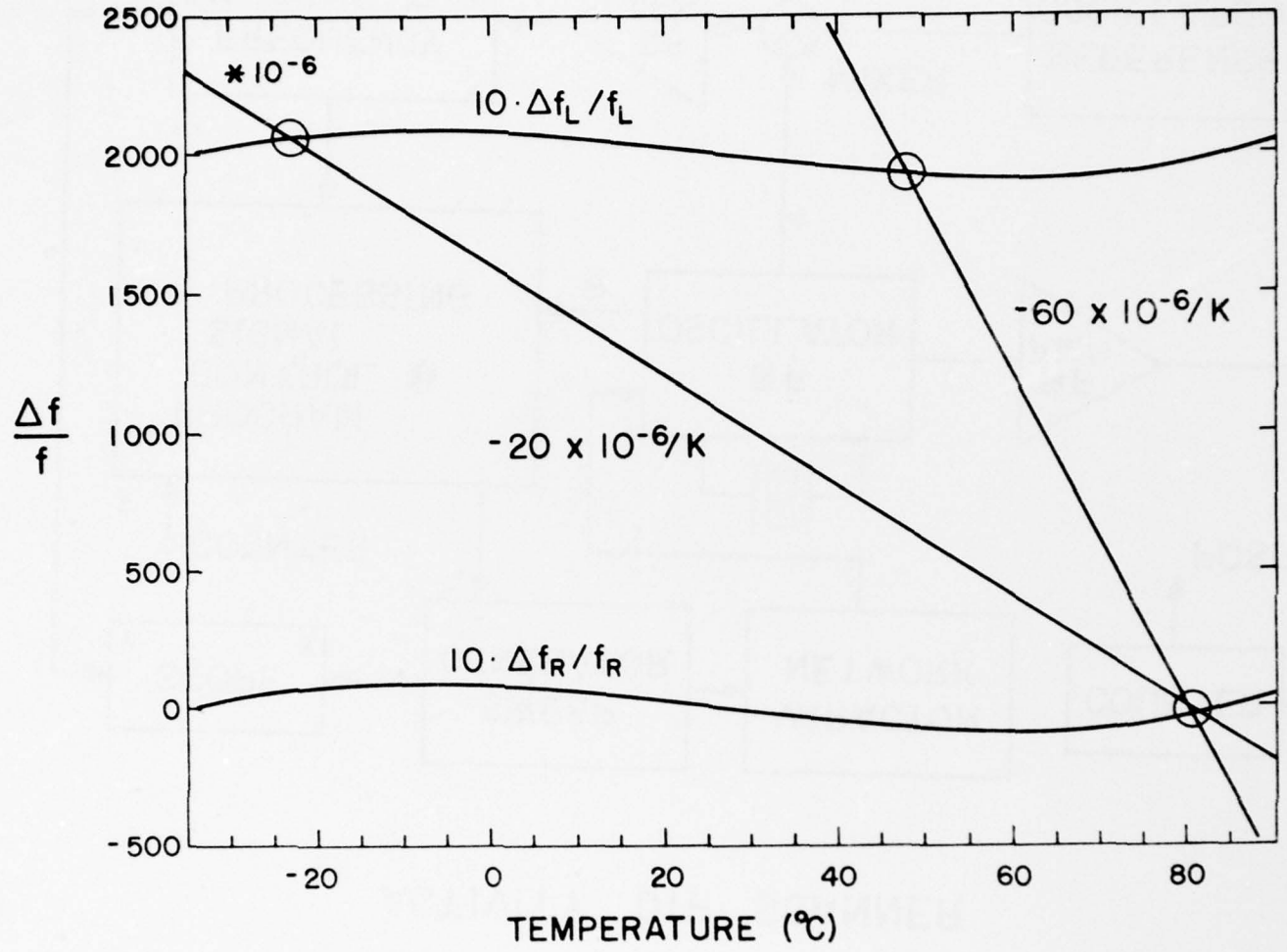

FIGURE 4. CONSTRUCTION FOR DEMONSTRATING CHANGE OF ACTIVITY DIP TEMPERATURE.

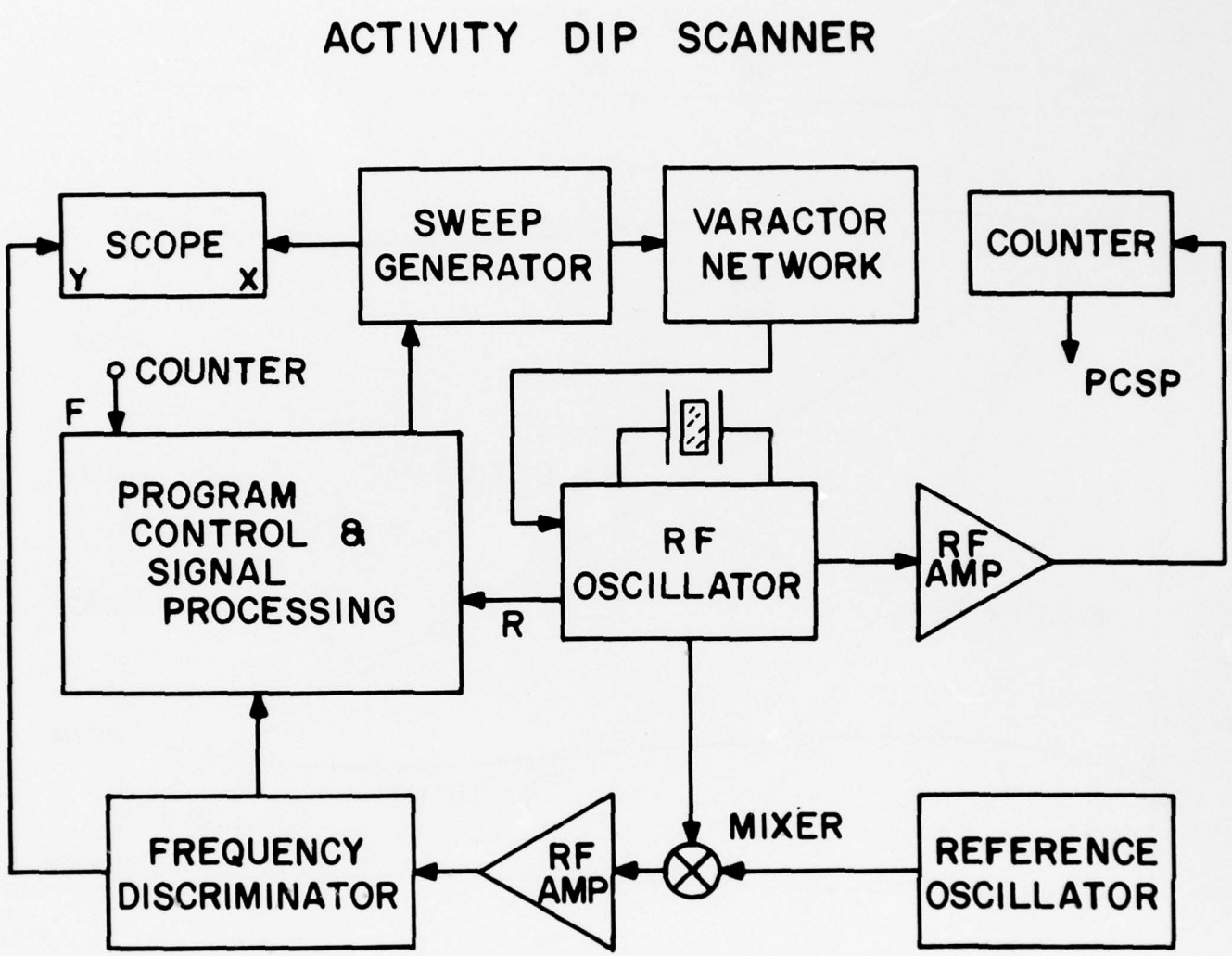

FIGURE 5. BLOCK DIAGRAM OF ACTIVITY DIP SCANNING EQUIPMENT.

It controls the sweep generator as well as receives resistance and frequency information for processing. A completely instrumented system would include provisions for acceptance/rejection of the unit for activity dips, evaluation of crystal parameters, output of results, and sequencing and control of input and output flow through the scanning apparatus on an assembly-line basis.

The sweep generator supplies the sawtooth voltage to both the X-axis of the scope and the varactor network. The varactor network responds to the voltage changes of the sweep generator and produces the variable C_L which is in series with the crystal unit under test.

The oscillator requires care in its design, but details will not be gone into here. One must be sure that the sought-for anomalies originate in the crystal and not the oscillator, so that unwanted frequency components must be strongly discriminated against. Depending on the type of crystal units and the stringency of the testing required, it may be adequate to use a standard CI Meter as the oscillator. We need only assume that the oscillator is such that it adjusts its frequency such that the crystal-load capacitor combination operates near or at its zero reactance point at f_L. Provisions for maintaining the drive level of the crystal constant, as C_L is varied, should also be considered in any embodiment of Figure 5. A schematic of an rf oscillator is shown in Figure 6.

The oscillator frequency output is mixed with a reference oscillator operating at the nominal frequency of the crystal under test. The difference frequency is applied to a frequency discriminator whose output is displayed on the Y-axis of the scope.

A system simpler than that of Figure 5 results from the elimination of the PCSP unit and operation of the sweep generator in a free-running mode.

The following instruments were used in a simple test setup for determining the feasibility of the method:

- Sweep generator: HP 3300A Function Generator
- rf oscillator: Crystal Impedance Meter TS-683/TSM (with low drive modification)
- Frequency discriminator: GR 1142-A Frequency Meter and Discriminator
- Reference oscillator: HP 5105A Frequency Synthesizer and HP 5110B Synthesizer Driver
- Mixer: HP 10514A Double Balanced Mixer
- Varactor network: The network shown in Figure 7 was used. Figure 8 shows the capacitance C_L measured between points A-B.

Examples of the type of outputs obtained with the simplified setup are shown in Figures 9, 10, and 11. These show line drawings taken from actual scope photos. In all cases, the temperatures T_i and power levels P_i follow the relations: $T_1 < T_2 < T_3$ and $P_1 < P_2 < P_3$. In Figure 9, temperature is

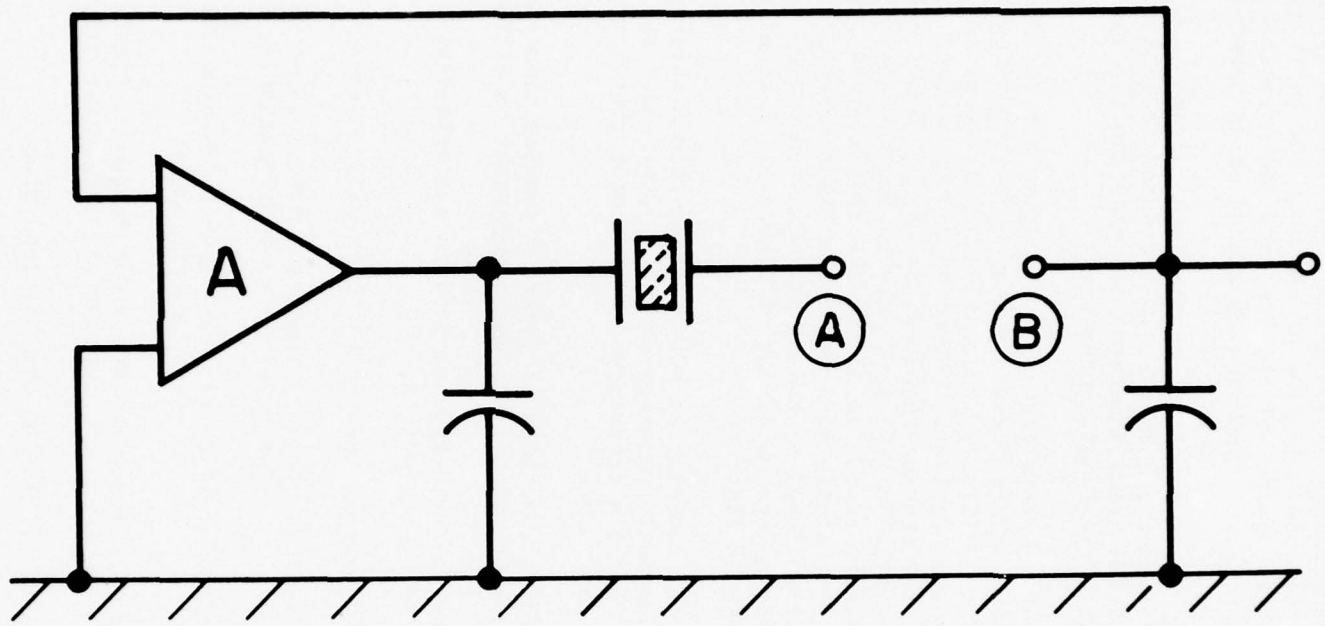

RF OSCILLATOR

FIGURE 6. SCHEMATIC OF RF OSCILLATOR.

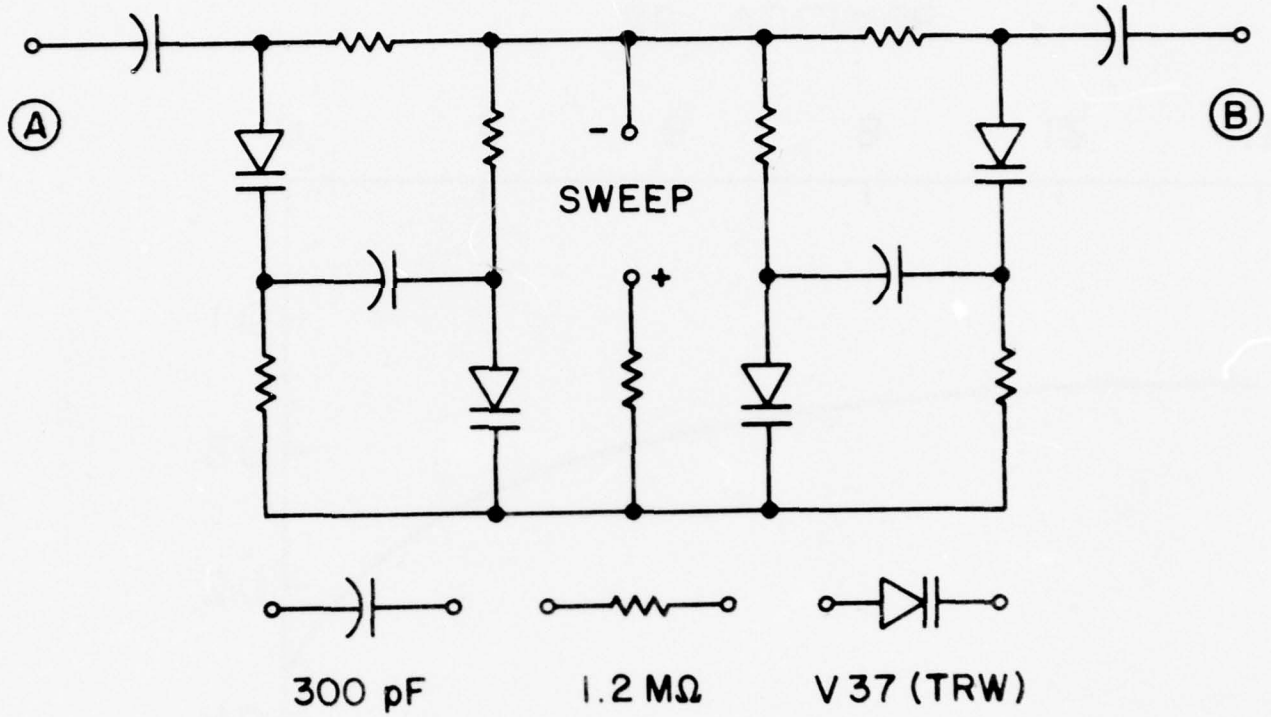

VARACTOR NETWORK

FIGURE 7. NETWORK FOR REALIZING ELECTRONICALLY VARIABLE LOAD CAPACITOR.

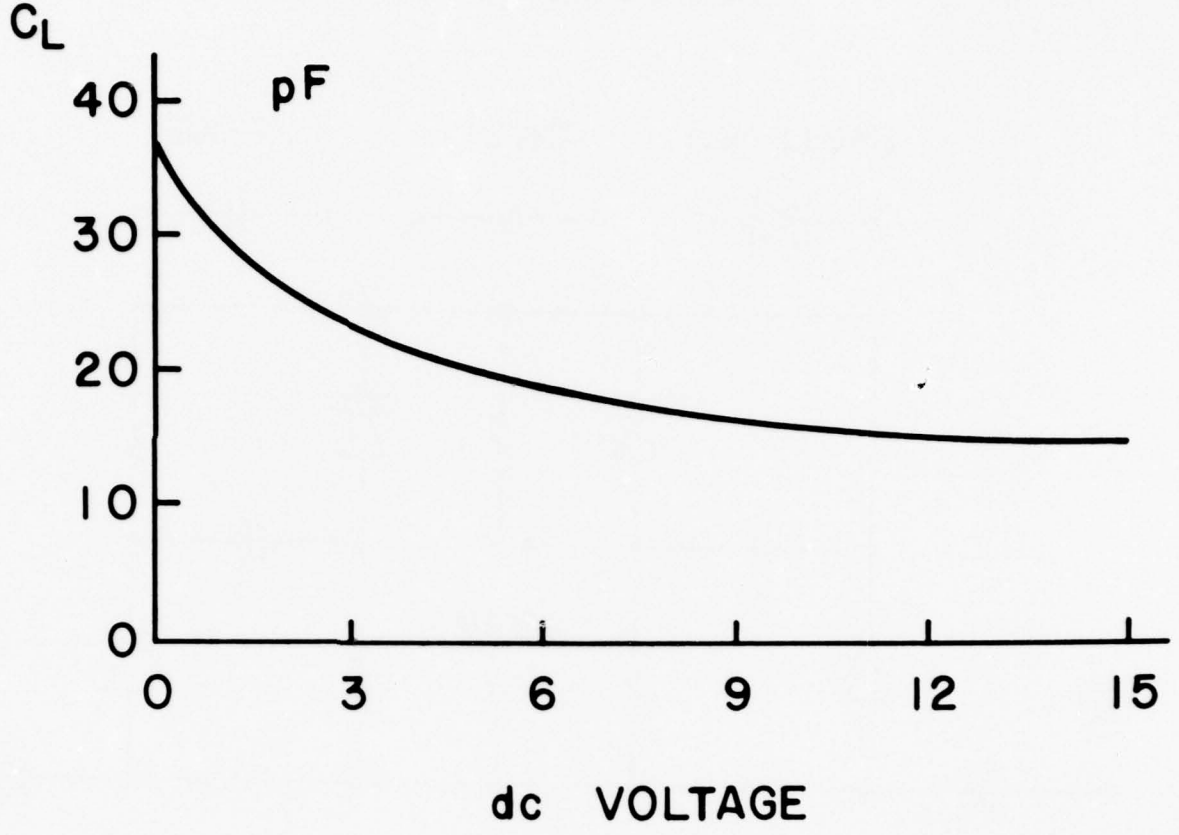

FIGURE 8. CAPACITANCE-VOLTAGE CHARACTERISTIC FOR THE NETWORK OF FIGURE 7.

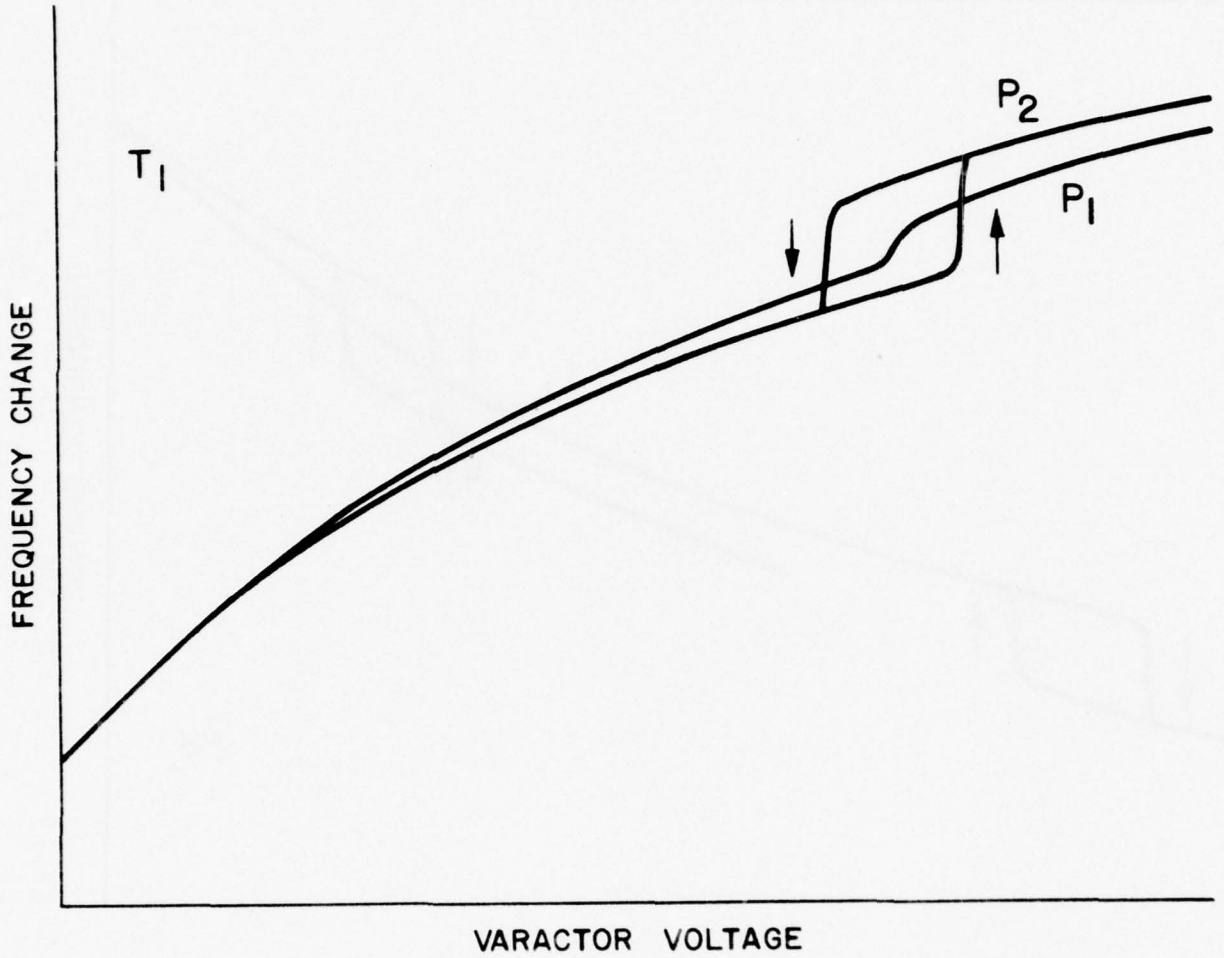

FIGURE 9. EXPERIMENTAL DETECTION OF ACTIVITY ANOMALY. TEMPERATURE CONSTANT.

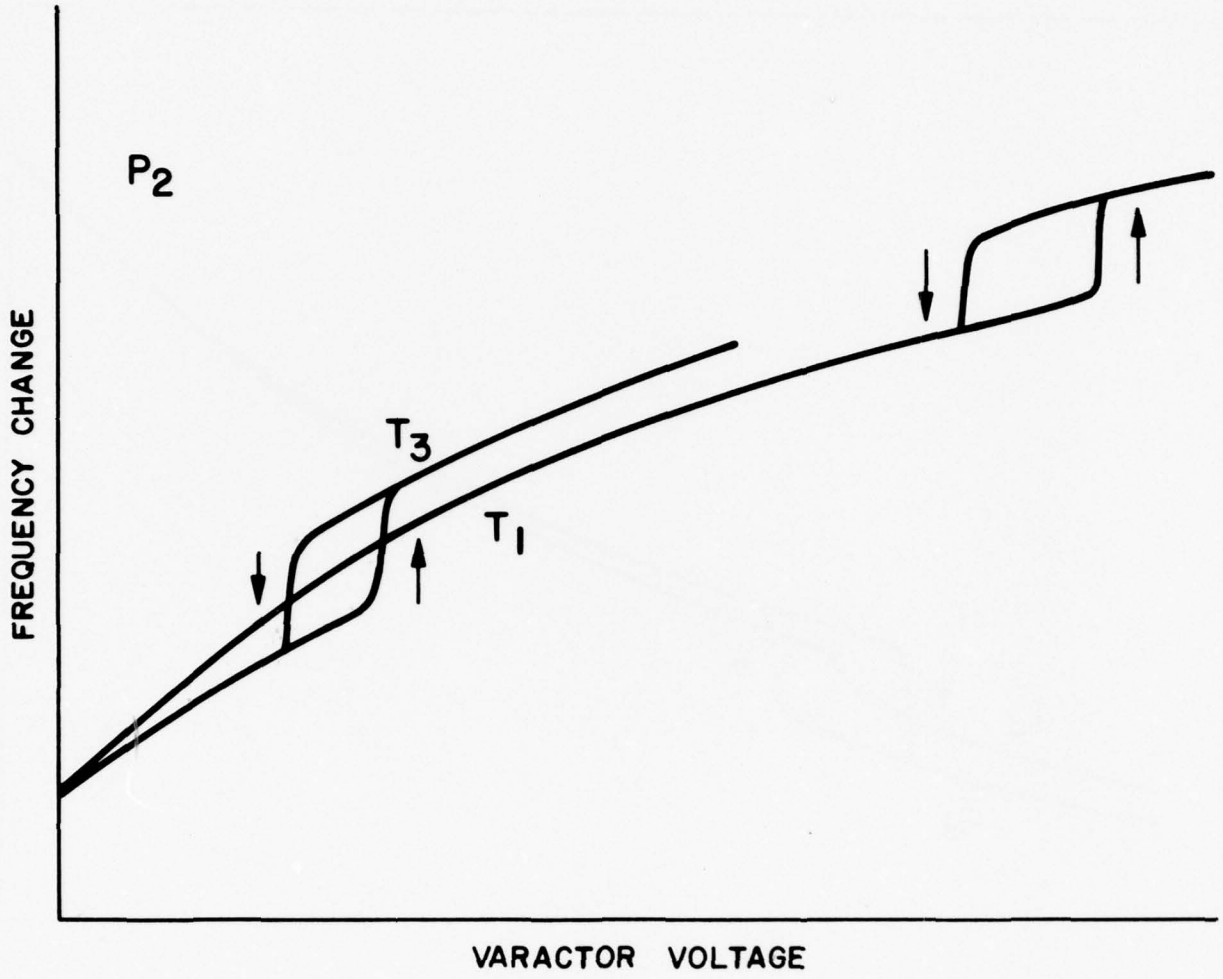

FIGURE 10. EXPERIMENTAL DETECTION OF ACTIVITY ANOMALY. POWER LEVEL CONSTANT.

FREQUENCY CHANGE VERSUS VARACTOR VOLTAGE AS FUNCTION OF TEMPERATURE AND POWER LEVEL

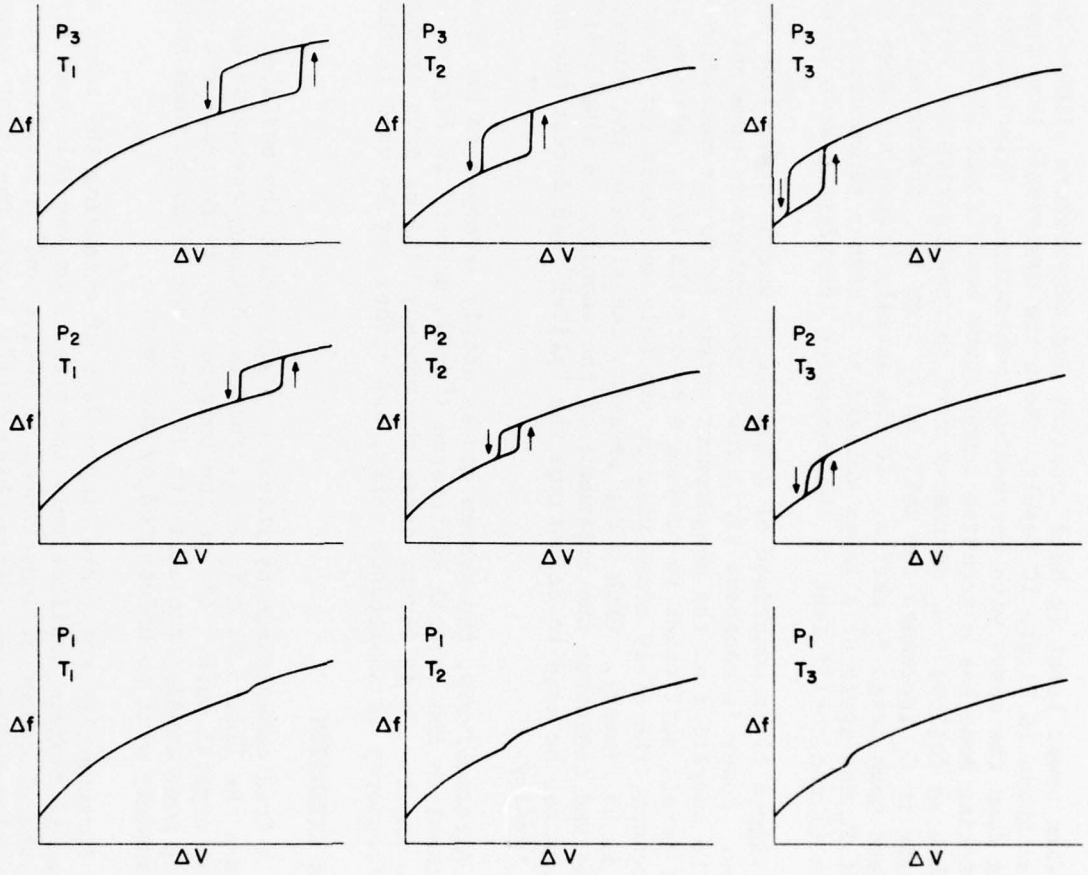

FIGURE 11. MONTAGE OF EXPERIMENTAL PLOTS OF FREQUENCY CHANGE VERSUS VARACTOR VOLTAGE.

held constant and power level is varied. At the low level P_1 the activity dip shows up as a sudden change in slope, although the curve remains a single-valued function. With increased drive, the dip is manifested by the presence of a hysteresis loop. Arrows indicate the direction of traverse as varactor voltage is swept back and forth.

When power level is held constant and temperature allowed to vary, curves such as those in Figure 10 result. Here the hysteresis loop position changes, moving down the curve with increasing temperature. This indicates that the interfering mode has a negative temperature coefficient of frequency. One may see this as follows: C_L decreases with increasing varactor voltage, and a decrease in C_L increases the shift of f_L from f_R. Therefore, high varactor voltages mean large f_L shifts. If the anomaly occurs at large varactor voltage at T_1 and again at a lower voltage at a higher temperature T_3, then (cf. Figure 4) the coefficient of the undesired interfering mode is negative.

Figure 11 is comprised of a montage of graphs taken from measurement photos. Power is constant along rows; temperature is constant along columns. For the operation of the measurement setup, it is not necessary to operate at power levels sufficient to produce a hysteresis loop. When no activity dip is present, the Δf-ΔV curve will be smoothly monotonic (it is not necessary that it be linear). With a dip present, the slope of the smooth curve is disturbed and indicates the existence of the anomaly. A simple differentiating network can be used to accentuate the "glitch" and detect the activity anomaly more readily.

Alternatively, the system can be simply arranged to use a voltage proportional to the crystal admittance ("grid current" in Figure 3 as the Y-axis scope input. In different cases the anomaly will be more prominent in either the frequency *or admittance shift*, and either may be used in the method.

RANGE EXTENSION

A load capacitance by itself can only shift the oscillator frequency between the limits $f_R \leq f_L \leq f_A$, that is, between resonance and antiresonance of the crystal unit. If, at the temperature of the test, the unwanted interfering mode causing the activity dip does not occur between these limits, then the anomaly will go undetected by the test.

Fortunately, there are simple ways of extending the range of the method. Figure 12 depicts qualitatively the effects on the pole-zero spectra resulting from the placement of inductances in series and in parallel with the crystal. The series inductance ("stretching coil") lowers the first reactance zero of the crystal while keeping the pole at f_A unaltered. Adding the varactor then permits the zero to be moved upward as with the crystal alone. In this manner, the frequency range below f_R can be scanned.

Placement of the inductance across the crystal does not change the reactance zero placement but shifts the pole at f_A to a higher frequency. A series varactor then permits the f_R zero to be shifted upward beyond f_A.

The series and parallel inductances can be electronically switched in and out of the circuit using PIN diodes controlled by the PCSP unit in the automatic measurement mode.

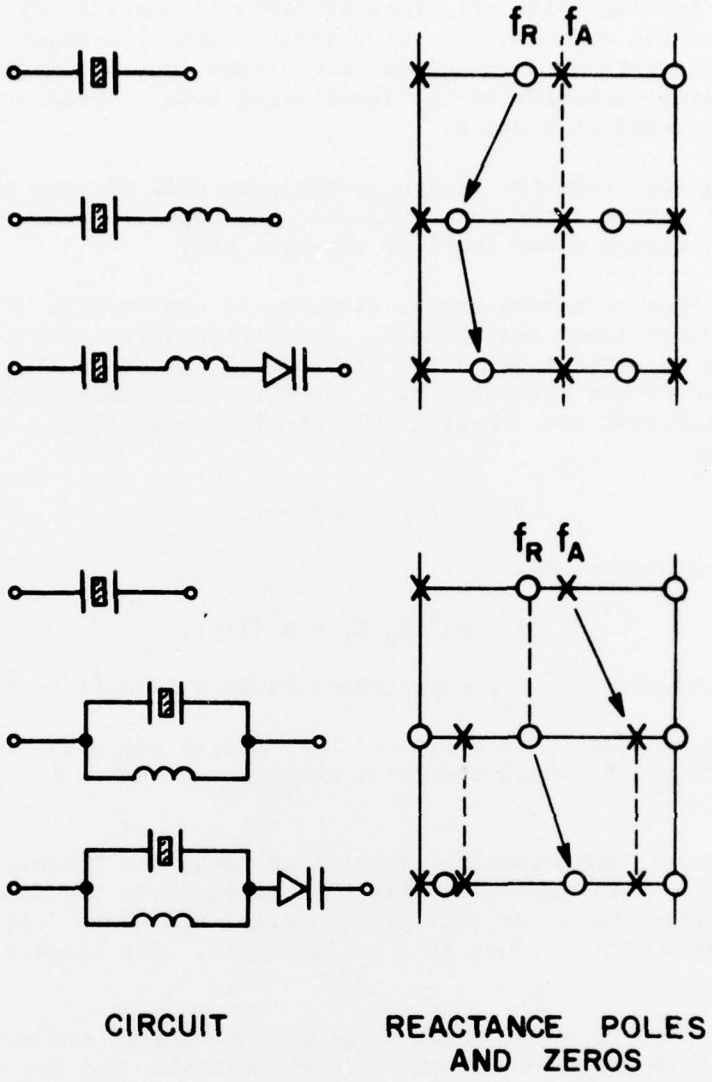

FIGURE 12. ALTERATION OF CRYSTAL POLE-ZERO LOCATIONS BY ADDITION OF CIRCUIT ELEMENTS.

From the point of view of network theory, the pole-zero shifts allowed are large; the limits imposed by the physics of the crystal vibrator are more stringent. Leaving aside all considerations of sensitivity of the system (Figure 5) on the detectability of activity dips, the major factors are the amplitudes of vibrator displacement and strain, and the magnitude and type of the coupling mechanism to the interfering mode. These are discussed briefly in appendices A and B.

For a given resonator design, experience will dictate practical ranges for the test system parameters, based on the type of modal interference encountered, design power level of crystal, etc.

The effects of adding series elements to the crystal is demonstrated in Figure 13, where input reactance X_{in} is plotted versus frequency. The frequency scale is normalized to the frequency f_s given in Figure 2; the abscissa is normalized to the reactance of C_o at f_s. The cases of series capacitor and series inductor are compared to that of crystal alone. The quantity β is defined as

$$\beta = C_o/C_L = \alpha/(1-\alpha), \tag{1}$$

for series capacitor, and

$$\beta = \omega_1^2 \, C_o \, L_L = \alpha/(1-\alpha), \tag{2}$$

for series inductor L_L; the capacitance ratio r is defined in Figure 2.

It is seen that C_L in series with a crystal pulls the reactance zero upward in frequency toward the pole, while L_L in series lowers the frequency of the zero.

In terms of the normalized quantities used, the frequency of the lower reactance zero of crystal plus series L_L is equal to the frequency of the upper reactance pole of crystal plus parallel L_L. This frequency is plotted against α for various values of r in Figure 14. For large r, $\Omega \simeq 1$ for $\alpha < \frac{1}{2}$.

The effects of parallel elements with a crystal are shown in Figure 15. The ordinate is normalized reciprocal susceptance, and the abscissa is frequency normalized to f_s. Here the poles are seen to change, and the zero remains fixed. Figure 16 graphs the frequency of the upper reactance zero of crystal plus series L_L combination, as function of α for various r values. This frequency is identical to that of the upper reactance pole of crystal plus parallel L_L. In Figure 16 the abscissas have been scaled to the quantity $(r/(r+1))^{\frac{1}{2}}$, whereas this factor is absent from Figure 14. Figure 14 and Figure 16 are almost (but not exactly) symmetric about the line $\alpha = \frac{1}{2}$. In Figure 16, for r large, $\Omega \simeq 1$ for $\alpha > \frac{1}{2}$.

CONCLUSIONS

A simple, rapid, electronic means of detecting the frequency/resistance anomalies known as activity dips has been described, with experimental confirmation. The method appears to be feasible to use in a number of possible ways:

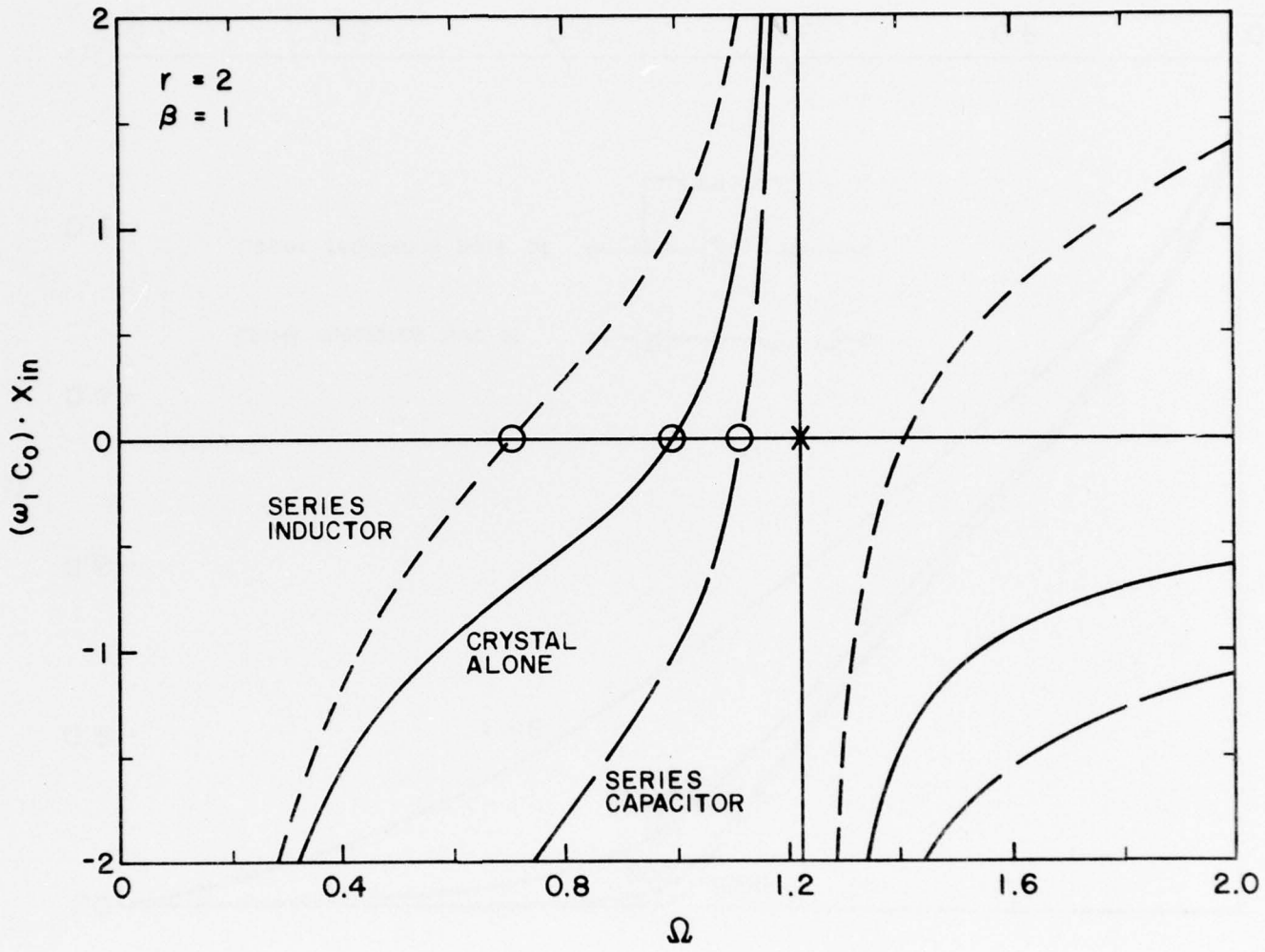

FIGURE 13. REACTANCE VERSUS FREQUENCY FOR SERIES ELEMENTS.

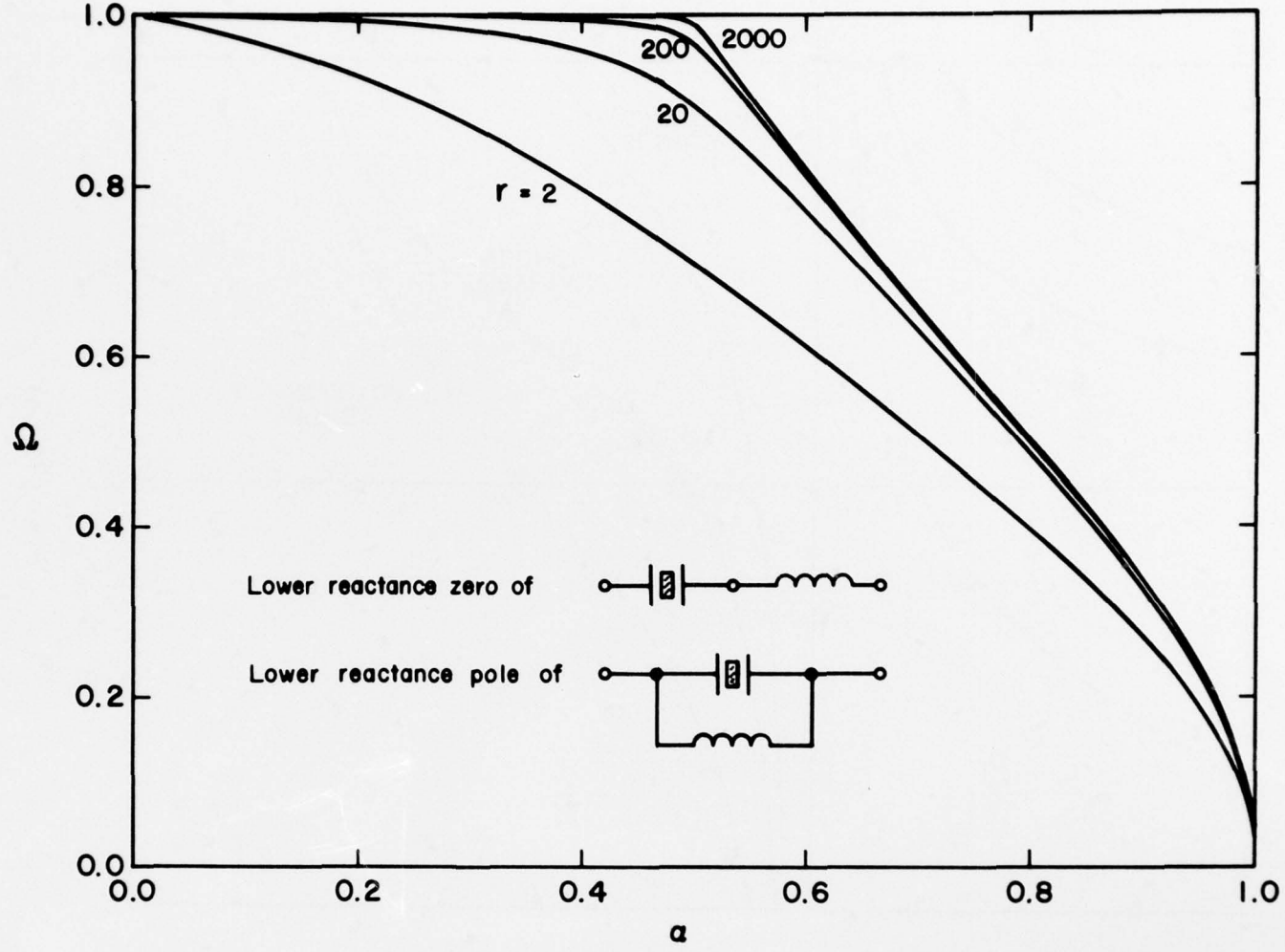

FIGURE 14. LOWER FREQUENCY VERSUS ALPHA FOR CRYSTAL/INDUCTANCE COMBINATIONS.

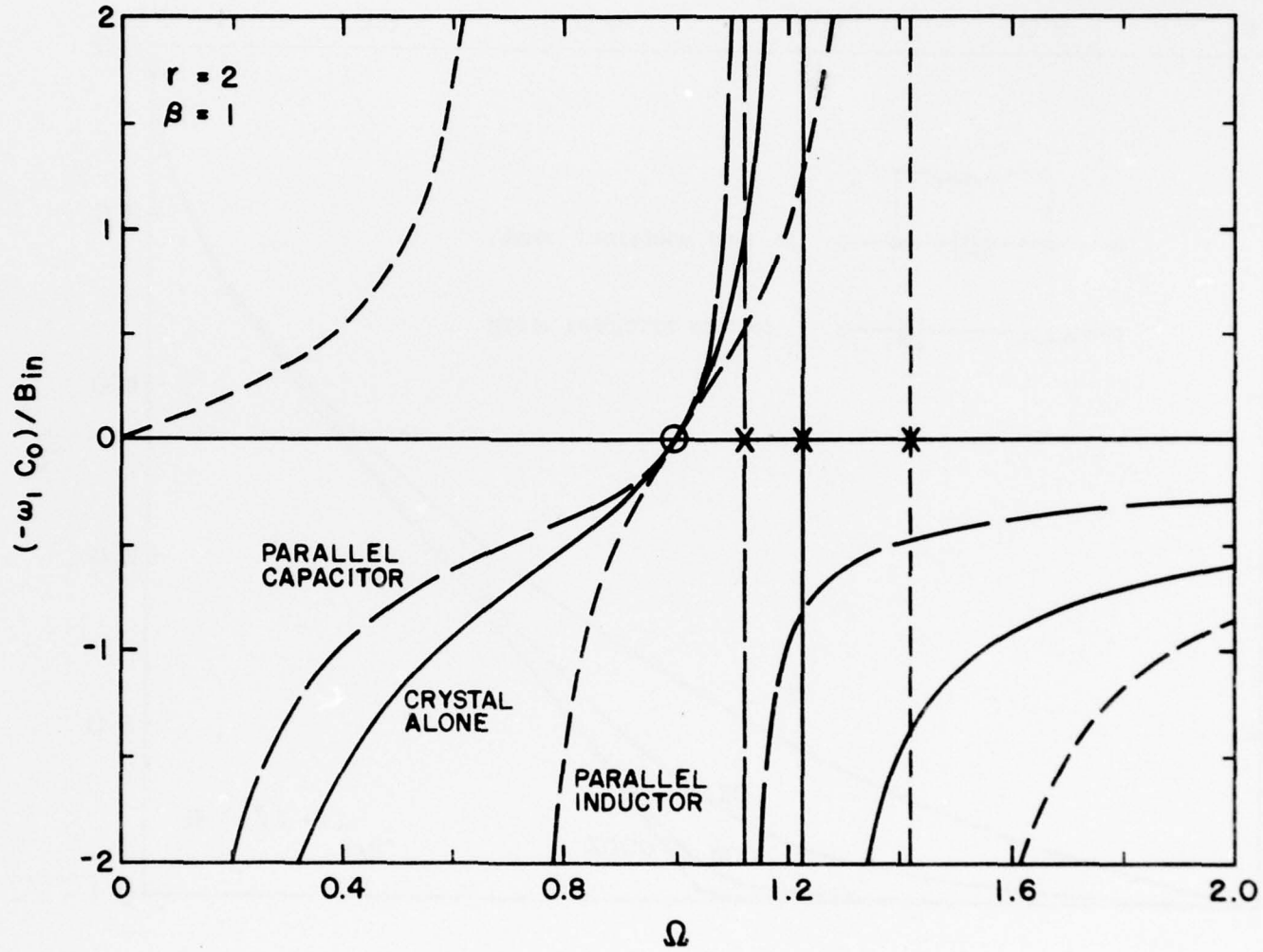

FIGURE 15. REACTANCE VERSUS FREQUENCY FOR PARALLEL ELEMENTS.

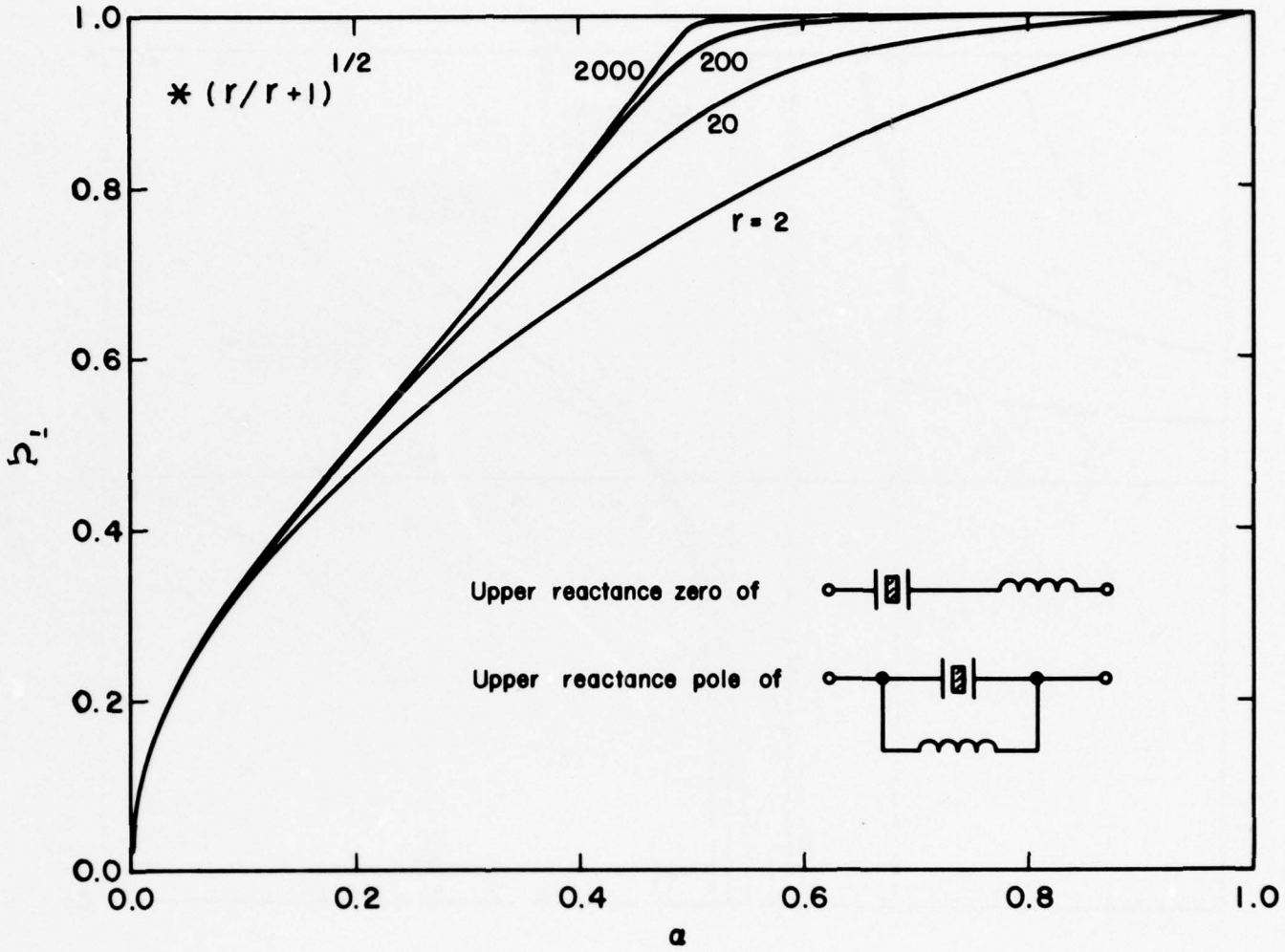

FIGURE 16. UPPER FREQUENCY VERSUS ALPHA FOR CRYSTAL/INDUCTANCE COMBINATIONS.

- As a rapid go-no go 100% inspection method for eliminating units having obvious and easily detected activity dips prior to making costly temperature runs.

- As a more highly instrumented method combined with measurements for determining the crystal C_o, C_1, R_1, L_1 parameters.

- As a hybrid method, combined with oven runs for interpolating between temperatures.

In this last variation, an oven is used, with or without the provisions for moving the pole and zero with inductors; but the oven is programmed to dwell at each of a number of fixed temperatures, say at 10°C intervals. At each fixed temperature, the varactor sweep method is used to search for dips. In this way, very onerous temperature runs in search of dips occurring over extremely small temperature intervals[13]* could be eliminated. The C_L in effect interpolates between fixed temperatures. See Appendix C for details.

REFERENCES**

1. E. Hafner, "Some Phenomena in VHF Crystal Units," Proc. 10th AFCS, May 1956, pp. 182-189.

2. H. Fukuyo, H. Yoshie, and M. Nakazawa, "The Unwanted Responses of Crystal Oscillator Controlled by AT-Cut Plate," Bull Tokyo Inst. Tech., No. 82, Sept. 1967, pp. 53-64; Proc. 21st AFCS, April 1967, pp. 402-419.

3. C. Franx, "On Activity Dips of AT Crystals at High Levels of Drive," Proc. 21st AFCS, April 1967, pp. 436-454.

4. A. F. B. Wood and A. Seed, "Activity dips in AT-Cut Crystals," Proc. 21st AFCS, April 1967, pp. 420-435.

5. I. Koga, "Anomalous Vibrations in AT-Cut Plates," Proc. 23rd AFCS, May 1969, pp. 128-131.

6. J. Birch and D. A. Weston, "Frequency/Temperature, Activity/Temperature Anomalies in High Frequency Quartz Crystal Units," Proc. 30th AFCS, June 1976, pp. 32-39.

7. A. Ballato and G. J. Iafrate, "The Angular Dependence of Piezoelectric Plate Frequencies and Their Temperature Coefficients," Proc. 30th AFCS, June 1976, pp. 141-156.

8. A. Ballato, "Doubly Rotated Thickness Mode Plate Vibrators," in Physical Acoustics: Principles and Methods (W. P. Mason and R. N. Thurston, eds.) Vol. 13, Chap. 5. New York: Academic Press, 1977.

9. E. P. EerNisse, "Calculations on the Stress Compensated (SC-Cut) Quartz Resonator," Proc. 30th AFCS, pp. 8-11, June 1976.

*See list of references on Page 23.

**AFCS: Annual Frequency Control Symposium, US Army Electronics Command, Fort Monmouth, NJ 07703.

10. J. A. Kusters and J. G. Leach, "Further Experimental Data on Stress and Thermal Gradient Compensated Crystals," Proc. IEEE, Vol. 65, No. 2, Feb. 1977, pp. 282-284.

11. J. A. Kusters, private communication, June 1977.

12. R. D. Mindlin, "Thickness-Shear and Flexural Vibrations of Crystal Plates," J. Appl. Phys., Vol. 22, No. 3, March 1951, pp. 316-323.

13. P. F. Godwin, Jr., and G. L. Snider, "Methods for Production Screening for Anomalous Responses in Quartz Crystals Intended for High Reliability Applications," Proc. 31st AFCS, in press, June 1977.

APPENDIX A

ESTIMATE OF NONLINEARITIES IN AT-CUT RESONATORS

Many of the most important kinds of activity dips arise from nonlinear processes. In order to get a feeling for the magnitudes that might be involved, we evaluate the ratio of the nonlinear to linear terms in the problem of intermodulation solved by Tiersten.[1,2]

From the nonlinear equation

$$c_{66}^{E} u_{1,22} + e_{26} \phi_{,22} - \rho^{\circ} \ddot{u}_1 = -\gamma[(u_{1,2})^3]_{,2} \tag{A-1}$$

we use the ratio

$$\zeta = \left| \frac{-\gamma[(u_{1,2})^3]_{,2}}{c_{66}^{E} u_{1,22}} \right| = \frac{3\gamma (u_{1,2})^2}{c_{66}^{E}} \quad . \tag{A-2}$$

as a measure of the size of the nonlinearity.

For the AT-cut,

$$\gamma = 13.7 \times 10^{11} \text{ Pa.} \tag{A-3}$$

Making use of the approximate linear solution for u_1, evaluated at resonance and at the center of the plate where $u_{1,2}$ is greatest, gives

$$\zeta = \frac{3\gamma \cdot |A_M|^2 \cdot \varkappa^2}{c_{66}^{E}} \quad , \tag{A-4}$$

where

$$|A_M| \simeq \frac{4}{\pi^2} \cdot \frac{1}{M^2} \cdot \frac{e_{26} V Q_M}{c_{66}^{E}} \quad . \tag{A-5}$$

For AT-cut quartz

$$c_{66}^{E} = 29.0 \times 10^{9} \text{ Pa} \; ; \; e_{26} = 0.095 \text{ C/m}^2 \quad . \tag{A-6}$$

Taking as an example a 10 MHz, fundamental resonator with Q of 500,000 and 1 mV applied voltage gives for the ratio of terms

$$\zeta \simeq 2.2 \times 10^{-8} \quad . \tag{A-7}$$

---

1. H. F. Tiersten, "Analysis of Intermodulation in Rotated Y-Cut Quartz Thickness-Shear Resonators," Proc. 28th AFCS, May 1974, pp. 1-4.
2. H. F. Tiersten, "Analysis of Intermodulation in Thickness-Shear and Trapped Energy Resonators," J. Acoust. Soc. Am., Vol. 57, March 1975, pp. 667-681.

APPENDIX B

RESONATOR AMPLITUDE WITH LOAD CAPACITOR

In consideration of how far f_L may realistically be pulled from f_R by additional circuitry, a knowledge of the displacement, stress, and strain fields of the resonator is required. Limiting ourselves to the single shear mode of an unbounded AT-cut plate allows these quantities to be computed simply.

For a plate of thickness 2h and applied voltage V, we have[1]

$$u_1 = \frac{-eh \sin\left(\frac{x_2}{h} X\right)}{\bar{c}\, X \cos X} \cdot a_2 \qquad \text{(B-1)}$$

$$S_6 = u_{1,2} = \frac{-e \cos\left(\frac{x_2}{h} X\right)}{\bar{c} \cos X} \cdot a_2 \qquad \text{(B-2)}$$

$$T_6 = e \cdot \left\{1 - \frac{\cos\left(\frac{x_2}{h} X\right)}{\cos X}\right\} \cdot a_2 \qquad \text{(B-3)}$$

$$a_2 = \frac{V/2h}{\left[1 - k^2 \frac{\tan X}{X}\right]} \cdot \qquad \text{(B-4)}$$

In the above,

$$e = e_{26}; \quad \bar{c} = \bar{c}_{66} = c^E_{66} + e^2_{26}/\varepsilon^S_{22}; \quad k^2 = k^2_{26} = e^2_{26}/\varepsilon^S_{22}\,\bar{c}_{66};$$

$$X = \frac{\pi}{2}\left(f/f^{(1)}_{Ao}\right); \quad f^{(M)}_{Ao} = M\sqrt{\bar{c}/\rho}\,/4h. \qquad \text{(B-5)}$$

The displacement u_1 is greatest at $x_2 = \pm h$, while the strain is largest at $x_2 = 0$. In terms of these maximum values we have

$$(u_1/h)_{\text{surface}} = (S_6)_{\text{center}} \cdot \frac{\sin X}{X} \cdot \qquad \text{(B-6)}$$

The resonance frequencies are obtained from the poles of a_2, that is, from the roots of

$$\tan X = X/k^2. \qquad \text{(B-7)}$$

---

1. A. Ballato, "Transmission-Line Analogs for Piezoelectric Layered Structures," Technical Report ECOM-4413, US Army Electronics Command, Fort Monmouth, NJ 07703, May 1976, 252 pp.

About these frequencies $f_{Ro}^{(M)}$, the presence of loss serves to limit the amplitude. The amplitude may be found by substituting

$$f_{Ro}^{(M)} \cdot (1 + j/2Q_M) \tag{B-8}$$

for $f_{Ro}^{(M)}$ in (B-1) to (B-4).

When C_L is used to pull the frequency to f_L, then the effect can be calculated by using

$$k_L^2 = k^2 (1 - \alpha), \tag{B-9}$$

with

$$\alpha = C_o/(C_o + C_L), \tag{B-10}$$

in place of k^2 in (B-7). This determines f_L. With the known value of f_L inserted into (B-1) to (B-4), the various amplitudes are determined away from resonance. As long as f_L is not too close to f_R, (B-8) need not be used for purposes of determining the effect of a load capacitor.

APPENDIX C

EFFECT OF C_o ERRORS IN C_1 MEASUREMENT

In the use of the electronic method for detecting activity dips, C_L is swept and used to perform a detection function. It was mentioned that the method could be used in conjunction with a procedure that measured the crystal parameters as well. One method of measuring C_1, the motional capacitance, consists in measuring f_R of the crystal, then inserting a series C_L and measuring f_L, the load frequency. The load frequency f_L is the frequency at which the crystal plus C_L combination exhibits zero reactance and low resistance. From Figure 2,

$$f_L^2 = f_s^2 \cdot (1 + \alpha/r). \tag{C-1}$$

Using the definitions of α and r and the approximations $f_s \simeq f_R$,

$$(f_L^2 - f_R^2)/f_R^2 \simeq 2(f_L - f_R)/f_R = 2\Delta f/f_R, \tag{C-2}$$

we obtain the commonly-used relation

$$C_1 \simeq 2\Delta f \cdot (C_o + C_L)/f_R. \tag{C-3}$$

If, as C_L is swept electronically, the quantity Δf is monitored, then C_1 can be computed continuously during the operation. It should be a constant, independent of C_L. When this is not the case, the trouble can be the presence of an activity dip; however, these are readily discerned as shown in the rest of this report. Another reason why the computed value of C_1 might vary with C_L is that an incorrect value for C_o is used in (C-3). The effect of errors in C_o is portrayed in Figure C-1. The abscissa is the modified ratio α' defined as

$$\alpha' = C_o'/(C_o' + C_L), \tag{C-4}$$

while the ordinate is normalized C_1 computed from C_o'. One sees that the effect on C_1 is gradual and not sharp as would be the case with an anomaly. The variation in apparent C_1 with C_L can be used by the microprocessor to correct C_o' to the true value C_o.

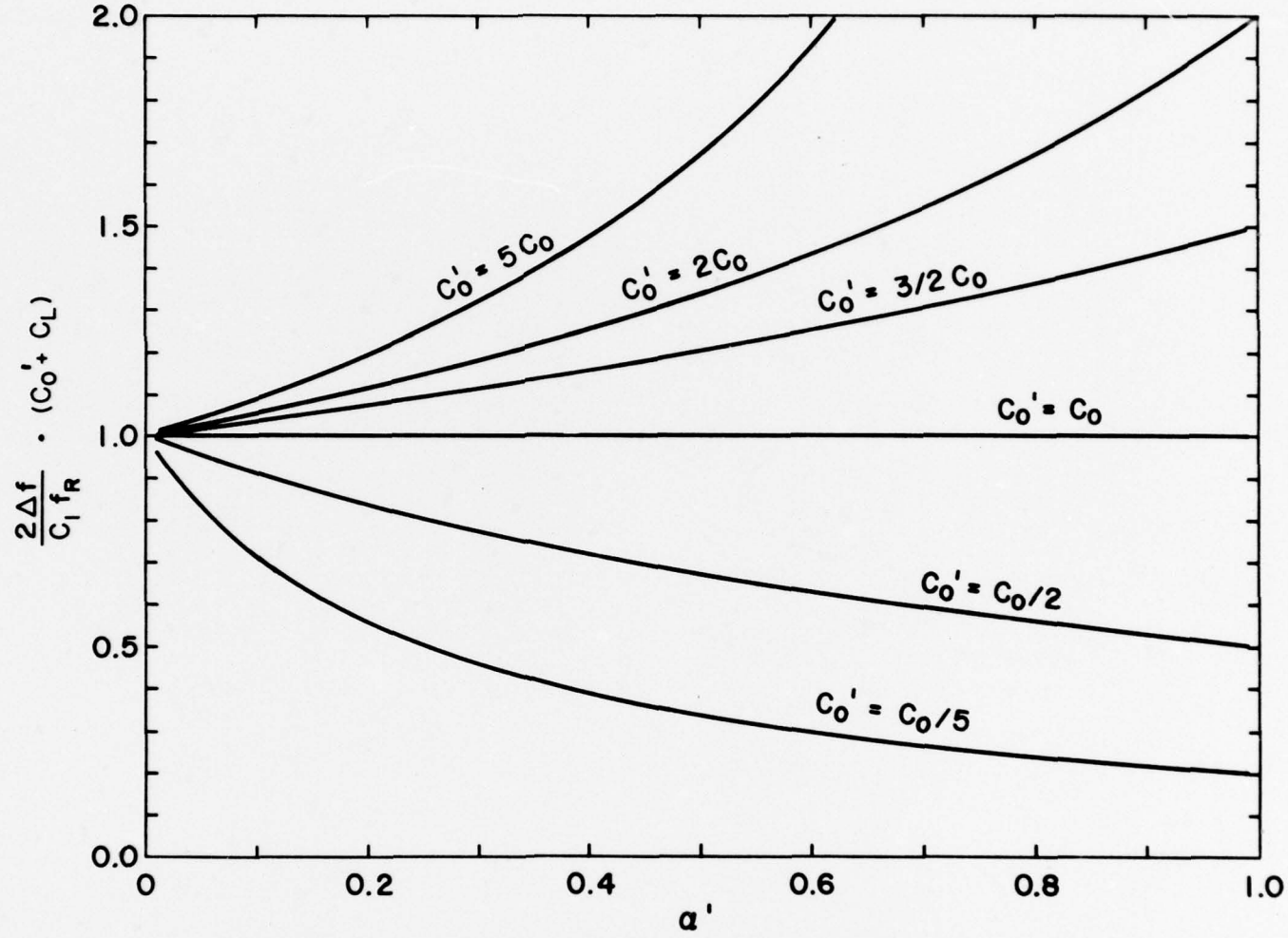

FIGURE C-1. APPARENT MOTIONAL CAPACITANCE VERSUS ALPHA PRIME.